Fuel Cell Fed EV Motor using Novel High Gain Landsman Converter with Energy Management System

Vendoti Suresh^{1*}, Kunche Gowthami², Balaga Ganesh³, Bollu Navaneeth Kumar⁴, Keta Ashok Kumar⁵

¹Assistant Professor, Department of Electrical & Electronics Engineering, Godavari Global University, Rajahmundry

²Assistant Professor, Department of Electrical & Electronics Engineering, Godavari Institute of Engineering and Technology
(A), Rajahmundry

³UG Scholar, Department of Electrical & Electronics Engineering, Godavari Institute of Engineering and Technology (A),
Rajahmundry

⁴UG Scholar, Department of Electrical & Electronics Engineering, Godavari Institute of Engineering and Technology (A),
Rajahmundry

⁵UG Scholar, Department of Electrical & Electronics Engineering, Godavari Institute of Engineering and Technology (A), Rajahmundry

(sureshvendoti.phd@gmail.com, gowthami12@giet.ac.in, balagaganesh2002@gmail.com, bollunavaneeth123@gmail.com, kethashokkumar@gmail.com)

*Corresponding Author: Vendoti Suresh, sureshvendoti.phd@gmail.com

Received: 10.06.2025 Accepted: 25.08.2025

Abstract- Fuel Cells (FC) are the greatest option for combining Electric Vehicles (EV) technology to improve performance because EVs have been experiencing a number of power quality concerns. The goal is to develop and optimize a FC system for an EV's Brushless DC (BLDC) motor in this research. This study focuses on Fuel Cell Electric Vehicles (FCEV), which combine FC technology and Energy Management Systems (EMS) in the best possible way to meet the electric motors' dynamic power demands. Nevertheless, the FC system produces less power, which is insufficient to power the EV. Therefore, a high gain Landsman converter is exploited in the research to enhance the FC's voltage. To deliver a controlled DC output voltage, a Proportional Integral (PI) controller is exploited and its parameters are optimized via Siberian Tiger Optimization (STO) algorithm. The extra power produced by the FCs is stored in a battery EMS, which is attached to the DC link via a battery converter. Bidirectional DC-DC (BDC) converter is exploited to interface different types of storage devices, includes batteries that supply electricity during periods of high demand. A PI controller manages the brushless DC motor's speed. Finally, the supply is given to the three phase (3ϕ) BLDC motor of EV through 3ϕ Voltage Source Inverter (VSI). To demonstrate the efficiency of proposed work, its performance is assessed utilizing MATLAB/Simulink. The obtained findings show that, the converter has the efficiency of 93.75% and THD of 1.11%, indicating that the FC powered PI controlled BLDC motor performs well for a range of speed and torque values.

Keywords FC, FCEV, BLDC motor, High gain Landsman converter, STO-PI controller.

1. Introduction

All nations in the world agree that rapidly generating clean energy is essential because of the severity of the global energy problem and environmental pollution [1-3]. The globe must switch to RES including wind, solar, hydropower, geothermal, and others in order to avoid these effects [4-6]. FCs are the most widely accepted of these because of their high power density, zero combustion, efficacy, and ecological

friendliness [7-9]. Due to its benefits, including zero emissions, recent advancements in FC technology have garnered a lots of attention [10-12]. The notable progress in FC and power electronics technology has facilitated the quick development of FCEVs [13, 14]. With the help of a catalyst, a FC is an energy conversion device that use oxygen (air) and hydrogen to generate electrical energy [15]. The FC produces

low voltage, which is enhanced by utilizing DC/DC converter and some of the conventional converters are discussed. One of the conventional converter is a Boost converter that provides a highest output voltage in order to maximize their outputs. It is widely used in FC applications because of their ability to function in the Continuous Conduction Mode (CCM) of current control mode. However, there are several issues with the high current ripples that occurred in this converter [16, 17]. Depending on the mode of operation, a Buck-boost converter is able to increase and reduce DC voltage. Nonetheless, it have restricted power conversion efficacy because of high voltage ratings on power switches [18]. The Cuk converter is utilized in many diverse applications, ranging from renewable energies to power factor adjustment. This converter have the advantages of non-pulsating output and input currents and minimal output voltage ripple. Nevertheless, this converter exhibits low conversion efficiency and high component stresses because it only has one power switch [19]. By connecting the SEPIC converter to a diode-capacitor voltage multiplier, produces a substantial voltage gain [20]. However, this converter generates less voltage gain and improperly uses input resources in the necessary way. As a result, this work develops a high gain Landsman converter to raise FC voltage.

The FC's low voltage is then stabilized using the PI controller, and an optimization algorithm is exploited to optimize its parameters. Particle Swarm Optimization (PSO) is a method is presented in [21] that requires extremely few algorithm parameters to be adjusted, making tuning easier. However, especially in high-dimensional search spaces, this approach might converge slowly to the global optimum. The design of Gray Wolf Optimization (GWO), which yields the maximum gains of the tuned PI controller and indicates improved control performance, is presented in [22]. However, the number of wolves and the highest iteration number are two parameters that affect the GWO algorithm's performance, and changing these values incorrectly result in less than ideal performance. In [23], a PI controller is developed whose parameters are improved by the Artificial Bee Colony (ABC) technique. It is the most effective method for enhancing supply quality, integrity, and reliability of the system; the controller lowers steady state error and considerably shortens settling times. Nevertheless, the ABC algorithm's search speed is rather slow, which results in prolonged computation durations. The Firefly optimization algorithm is developed in [24], which improves the stability and overall system's performance. However, the implementation of this algorithm is very complex. To overcome this issues, this paper uses Siberian Tiger optimization algorithm for tuning the parameters of PI controller. Primary contribution of this work are,

- FC is designed and used as a clean energy source for the EV, assuring zero emissions and stable operation.
- A novel modified Landsman converter with a switched reactive network (SRN) is presented to increase the low FC voltage, resulting in higher voltage gain and efficacy.
- ➤ PI controller are optimized using STO method, which achieves faster convergence, shorter settling time, and increased system stability.
- To charge and discharge the battery effectively, allowing for seamless energy management and uninterrupted supply during FC operation under low power situations, a BDC converter is implemented.
- The 3ϕ VSI is used to convert regulated DC into AC with higher power quality, whereas PI control assures proper switching and motor stability.
- \triangleright A 3 ϕ BLDC motor is modelled and driven using optimised control, resulting in steady speed and torque response under dynamic load fluctuations.

2. Proposed Methodology

Currently, there is an ecologically development of energy technology that uses FCs, which is significantly increased. This paper proposes FC served EV motor using high gain landsman converter with EMS as revealed in Figure 1.

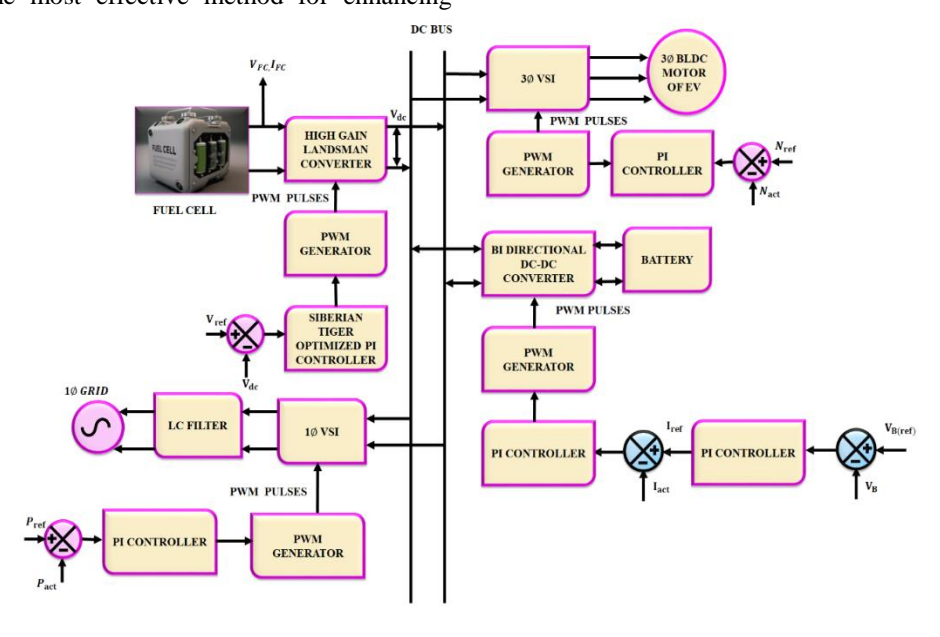


Fig. 1. Block diagram of developed research.

At first, the low voltage of FC is enhanced by exploiting high gain Landsman converter. The PI controller, to stabilise the FC voltage, and parameters are efficiently tuned via the STO algorithm. The surplus energy from FC is stowed in a battery and BDC converter is employed to execute charging/discharging operation of battery. The 3ϕ receives output of proposed converter and converts DC to AC supply. The PWM generator generate pulses for VSI's better switching operation and PI controller is exploited to regulate the motor's speed. Then, the output of VSI is passed into the 3ϕ BLDC motor of EV. If there is no power from FC then the battery is utilized to give supply to DC bus. Also, the converter's output is then subjected into 1ϕ VSI, converting the source into AC. The PWM generator is used for better operation of VSI and PI controller is exploited to control the inverter. The supply is then sent to 1\phi grid via an LC filter, which removes unwanted harmonics. It assures the uninterrupted supply is delivered to the grid.

2.1. Modelling of Fuel Cell

FCs are sustainable power sources that use electrolysers to transform hydrocarbons into electrical energy (DC). A FC stack is formed by sending hydrogen fuel via the other side of an FC and connecting multiple FCs in parallel and series. Figure 2 depicts the FC's equivalent circuit, which consists of resistance and a voltage source diode. The FC's cell voltage is expressed in (1)

$$V_{f} = E - V_{a} - V_{b} - V_{c}$$

$$\text{NAln}(^{If_{c}}/_{I_{o}}) \xrightarrow{\text{If}_{c}}$$

$$\text{E}_{\text{oc}} \xrightarrow{\text{RINT}} \xrightarrow{\text{If}_{c}}$$

$$\text{Vf}_{c}$$

Fig. 2. Equivalent circuit of fuel cell.

The open circuit thermodynamic voltage is

$$E = 1.229 - 0.00085(T - 298.15) + 0.00004308T(ln(PH2) + 0.5ln(P02))$$
(2)

The combination of cathode and anode voltage is known as activation voltage, which is expressed as

$$V_a = -[A_1 + A_2T + A_3Tln(CO_2) + A_4Tln(I_{fc})]$$
 (3)

The ohmic voltage is

$$V_b = \left(I_{fc}R_a + I_{fc}R_b\right) \tag{4}$$

The concentration voltage is

$$V_c = -\frac{RT}{nF} ln \left(1 - \frac{J}{lm} \right) \tag{5}$$

The open circuit voltage is estimated as

$$E_{oc} = E_n K_c \tag{6}$$

The collected current via the FC is calculated as

$$I_0 = \frac{ZFK(PH_2 + PO_2)}{R_{in}h} e^{-\Delta G/R_{in}T}$$
 (7)

Here T stands temperature, R_{in} stands internal resistance. Then, the low voltage of FC is given to the high gain Landsman converter.

2.2. High Gain Landsman Converter

As seen in Figure 3, the developed converter is designed by modifying a traditional landsman converter, which uses a switched reactive network (SRN) to produce high voltage gain. The SRN boosts the converter's overall voltage gain by diodes and D_{ν}), (D_i) inductor (L_i) and capacitor (C_i) . One important component in the circuit that raises the voltage on load is the capacitor C_i . It is operated in 2 modes: shoot-through ($0 \text{ to } DT_S$) and nonshoot-through $(DT_S - T_S)$ stage, where D is the duty ratio and $T_{\rm S}$ is the duration of one shifting cycle, because the developed converter is regulated through a single switch S. The following assumptions are made when discussing the working principle of developed converter in continuous conduction mode: At first, each inductors (L_1, L_2) and L_i are demagnetized, and capacitors (C_1 and C_2) are fully charged.

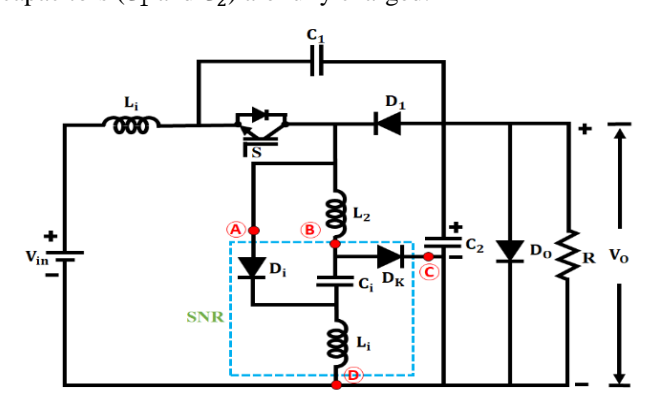


Fig. 3. Circuit diagram of developed converter.

Shoot-through mode

In shoot-through mode, capacitor C_1 reverse biases diode D_1 . Through switch S and diode D_i , input supply V_{in} charges inductor L_1 and L_i in series. Also, the input supply charges the C_i through D_i and the L_2 through diode D_k . C_1 charges C_2 throughout the same time period. Figure 4 displays each loop's current path.

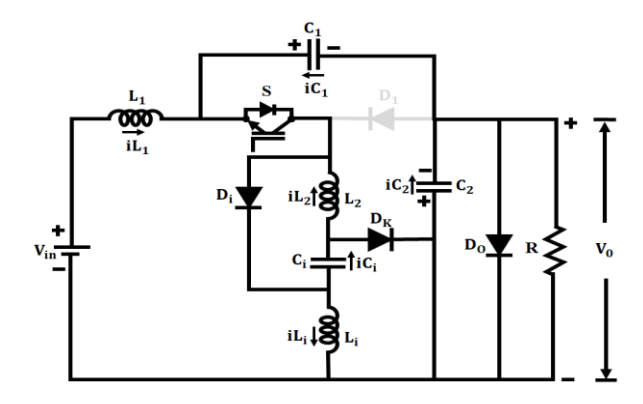


Fig. 4. Circuit of shoot-through mode.

Non-shoot through mode

In this mode, C_1 is charged in non-shoot mode by input supply V_{in} and inductor L_1 . As illustrated in Figure 5, the load obtains energy from the L_2 , L_i and C_i with assistance of diode D_k .

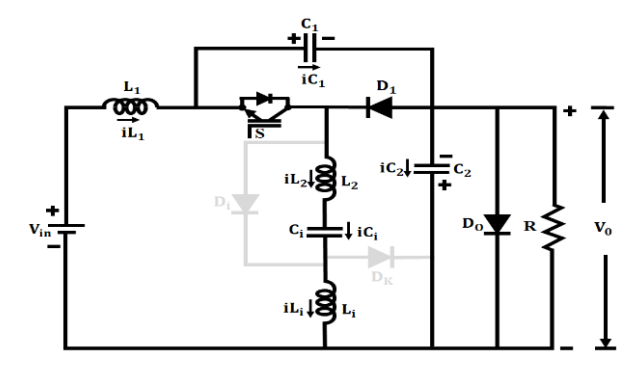


Fig. 5. Circuit of non-shoot through stage.

Figure 6 depicts the distinctive waveforms of each component throughout the non-shoot and shoot-through periods. The corresponding voltage formula in both shoot and non-shoot stages is as follows:

$$V_{in} - V_{L1} - V_{Ci} - 4V_d = 0 (8)$$

$$V_{in} - V_{L1} - V_{Li} - 4V_d = 0 (9)$$

$$V_{in} - V_{L1} - V_{L2} - 4V_d = 0 (10)$$

$$V_{C1} - V_{L2} - V_{C2} - 3V_d = 0 (11)$$

$$V_{C2} = -V_0 (12)$$

$$\begin{cases} V_{in} - V_{L1} - V_{C1} - V_{O} - V_{d} = 0 \\ -V_{L2} + V_{Ci} - V_{Li} + V_{O} - 3V_{d} = 0 \end{cases}$$
 (13)

The voltage second balance law is applied to L_1 , which is given as,

$$(V_{in} - V_{Ci} - 4V_d)D + (V_{in} - V_{C1} - V_O - V_d)(1 - D) = 0$$
 (14)

The above equation becomes

$$V_O = \frac{V_{in} - V_{CID} - V_{d}(3D+1)}{(1-D)} - V_{C1}$$
 (15)

The corresponding voltage through both inductors L_2 and L_i when both inductors are same, which is expressed as

$$V_{L2} = V_{Li} = \frac{V_{Ci} + V_O - 3V_d}{2} \tag{16}$$

The voltage second balance law is employed to L_i and L_2 , which is calculated as,

$$(V_{Ci} - 8V_d)D + \left(\frac{V_{Ci} + V_O - 3V_d}{2}\right)(1 - D) = 0 \quad (17)$$

$$V_{Ci} = -\left(\frac{1-D}{1+D}\right)V_0 - \left(\frac{3+13D}{1+D}\right)V_d \tag{18}$$

$$(V_{C1} + V_O - 3V_a)D + \left(\frac{V_{Ci} + V_O - 3V_a}{2}\right)(1 - D) = 0$$
 (19)

$$V_{C1} = -\left(\frac{1+D}{2D}\right)V_O - \left(\frac{1-D}{2D}\right)V_{Ci} + \left(\frac{1+D}{2D}\right)3V_d \tag{20}$$

The voltage gain estimated from equations (4), (6) and (7)

$$\frac{V_O}{V_{in}} = -\left(\frac{1+D}{1-D}\right) + \left(\frac{43D^3 + 27D^2 - 7D - 1}{4(1+D)(1-D)}\right) \tag{21}$$

The voltage at output of converter (In the circuit element's ideal condition $(V_d = 0)$) is

$$\frac{V_O}{V_{in}} = -\left(\frac{1+D}{1-D}\right) \tag{22}$$

The input and output power is equated then the output current of converter is

$$\frac{I_O}{I_{in}} = -\left(\frac{1-D}{1+D}\right) \tag{23}$$

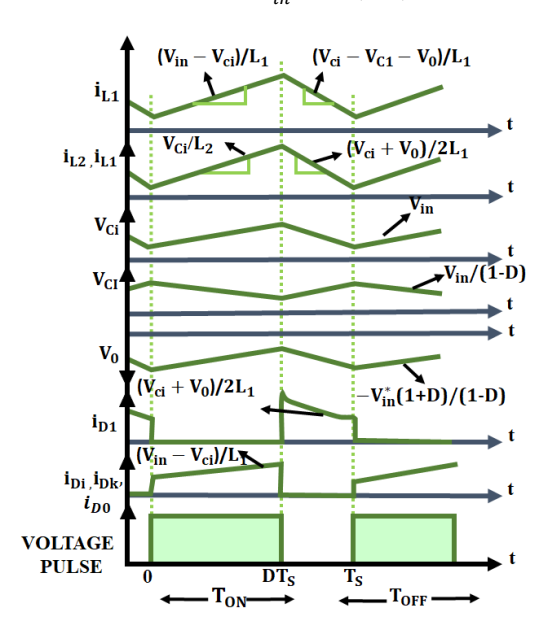


Fig. 6. Waveform of developed converter.

The SRN extends the voltage gain of the Landsman converter with an auxiliary path that provides a diode—capacitor—inductor storage path. During the shoot-through interval, the SRN permits the input source to simultaneously charge multiple reactive elements which store more energy. The stored energy is delivered in series with the input, which multiplies a voltage at the output during the non—shoot-through interval. The dual energy transfer mechanism allows the step-up ratio to exceed that of the Landsman converter while sharing the current stress amongst the respective components, providing a more efficient and reliable approach. Thus, the SRN provides an alternative method of providing gain while reducing device stress.

2.3. Siberian Tiger Optimized PI Controller

A PI controller is implemented in developed work for preserving a constant output by varying the control input. For optimal performance of system, the proportional gain (K_p) and integral gain (K_i) PI controller parameters has tuned. STO algorithm is exploited to efficiently optimize the parameters depending on a predefined performance criterion, like diminishing the settling time or Integral of absolute error (IAR). To detect the optimal values for K_p and K_i , that reduce a specific objective function, which is estimated as,

$$F(K_p, K_i) = \int_0^T |e(t)| dt$$
 (24)

Where the error among the actual and desired output of the system over time T is denoted as e(t).

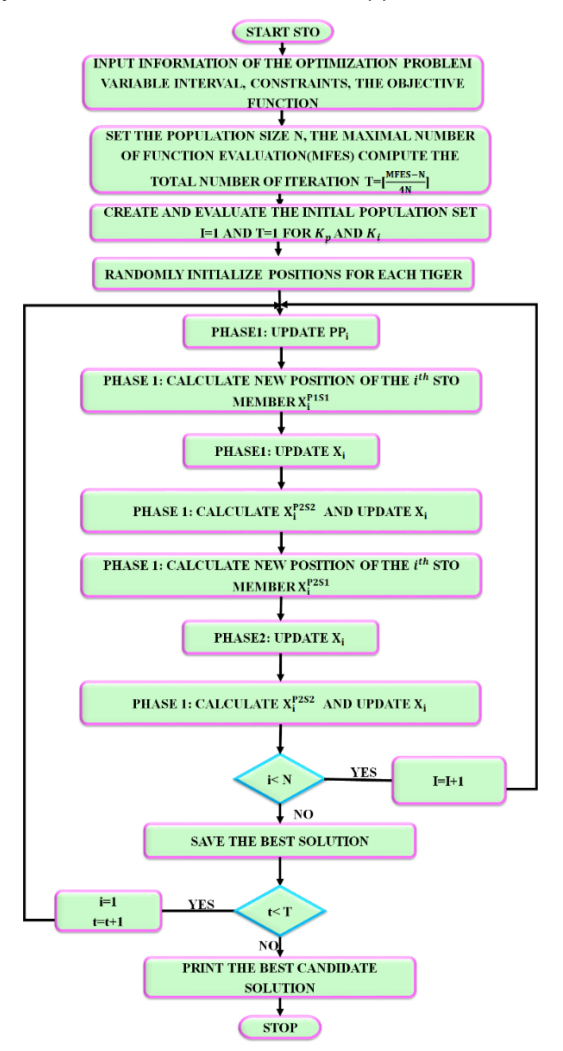


Fig. 7. Flowchart of STO-PI controller.

Initialization

Representation of population

Each Siberian tiger in the population indicates a candidate solution for the parameters of PI controller, which is calculated as

$$X_i = \left[K_{p,i}, K_{i.i} \right] \tag{25}$$

Where, i^{th} tiger's position is X_i .

Initial Position

The initial position of the tigers are randomly produced within specific bounds

$$K_{p,i} \in lb_p, ub_p, K_{i.i} \in lb_i, ub_i$$
 (26)

Where, upper and lower bounds for K_p and K_i is ub and lb.

Phase 1: Prey Hunting

Stage 1- Selection and Attack: Update positions based on better solutions (prey):

Find better solutions

$$PP_i = \{X_k | F_k < F_i\} \cup \{X_{hest}\}$$
 (27)

Randomly select a prey TP_i from PP_i .

$$X_{P1S1,i} = X_i + r. (TP_i - X_i)$$
 (28)

Stage 2-Chase: Refine the position based on a local search

$$X_{P1S2.i} = X_{P1S1.i} + \epsilon \cdot (X_{best} - X_{P1S1.i})$$
 (29)

Where small adjustment factor is indicated as ϵ .

Phase 2: Fighting with bears

Stage 1- Ambush: Randomly select another tiger (bear) to update positions

$$X_{P2S1,i} = X_i + r.(X_K - X_i)$$
 (30)

Stage 2-Combat-Make small adjustments

$$X_{P2S2,i} = X_{P2S1,i} + \delta \cdot (X_{best} - X_{P2S1,i})$$
 (31)

Where minor perturbation factor is represented by δ .

Acceptance criterion

Update the position when the objective function improves:

$$X_{i} = \begin{cases} X_{P2S1,i} & if F_{P1S2,i} < F_{i} \\ X_{i} & otherwise \end{cases}$$
 (32)

Repeat the above stages until a stopping criterion is met (like satisfactory error level or highest number of iterations). The use of the STO algorithm for tuning a PI controller permits for an effective exploration of parameter space, led to better performance as shown in Figure 7.

2.4. Bidirectional Battery Converter

The battery is coupled to DC bus via a BDC converter, which allows for charging and discharging built on system conditions. The control method is based on the FC's SOC and a real-time power balance with the load and the grid. When the FC generates excess power, the converter enters charging mode to store it in the battery. If the FC power is inadequate to meet load demand, the converter switch to discharging mode, allowing battery to power the DC bus. An idle mode is also incorporated, in which the converter remains inactive when the FC alone to meet the load need. A cascaded PI structure is used to control BDC converter, where the inner PI regulates the current to have a fast dynamic response while the outer PI is responsible for achieving the battery-side objective, such as SOC and voltage, by establishing the reference for the inner current loop. These rule-based mode-switching criteria ensure smooth energy flow, prevent battery overcharging or over-discharging, and maintain stable system operation with extended battery life.

2.5. Three Phase BLDC Motor of EV

Armature winding and torque equations are employed in the modeling of a 3ϕ BLDC motor. Figure 8 illustrates the

analogous circuit of a BLDC motor with a trapezoidal back EMF. Rotor position determines the back EMF and torque constant. As the voltage calculations based on the back EMF within the armature windings are

$$\begin{bmatrix} V_1 \\ V_2 \\ \vdots \\ V_n \end{bmatrix} = R \cdot \begin{bmatrix} I_1 \\ I_2 \\ \vdots \\ I_n \end{bmatrix} + L \cdot \begin{bmatrix} \dot{I}_1 \\ \dot{I}_2 \\ \vdots \\ \dot{I}_n \end{bmatrix} + \begin{bmatrix} e_1 \\ e_2 \\ \vdots \\ e_n \end{bmatrix}$$
(33)

Where V_1, V_2, \ldots, V_n represents provided voltage to each phase, and n denotes phase number. L denotes inductance, R stands armature winding resistance, I stands phase current, and e stands back EMF. The phase angle (360/n) between each phase's back EMFs is as follows.

$$\begin{bmatrix} e_{1}(t) \\ e_{2}(t) \\ \vdots \\ e_{n}(t) \end{bmatrix} = \begin{bmatrix} K_{en}(\theta) \\ K_{en}\left(\theta - \frac{2\pi}{n}\right) \\ \vdots \\ K_{en}\left(\theta - \frac{2\pi}{n}(n-1)\right) \end{bmatrix} . \omega(t)$$
(34)

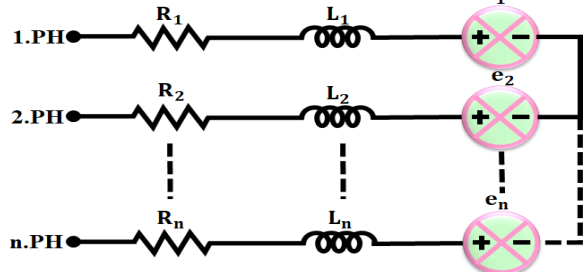


Fig. 8. Circuit of a BLDC motor.

Where one phase of the n-phase motor's back EMF constant is denoted as K_{en} and each phase's torque at output is

$$\begin{bmatrix}
T_{1}(t) \\
T_{2}(t) \\
\vdots \\
T_{n}(t)
\end{bmatrix} = \begin{bmatrix}
K_{Tn}(\theta) \\
K_{Tn}(\theta - \frac{2\pi}{n}) \\
\vdots \\
K_{Tn}(\theta - \frac{2\pi}{n}(n-1))
\end{bmatrix} \cdot \begin{bmatrix}
I_{1}(t) \\
I_{2}(t) \\
\vdots \\
I_{n}(t)
\end{bmatrix}^{(-1)} (35)$$

Here phase of the n-phase motor's torque constant is indicated by K_{Tn} . Overall torque at output is

$$T_e = T_1 + T_2 + \dots + T_n \tag{36}$$

Where total torque at output is represented as T_e .

3. Results and Discussion

This section examines the characteristics of FC, proposed converter and controller with appropriate waveforms. It is modelled and simulated in MATLAB/Simulink R2023a on a desktop computer equipped with an Intel i7 3.4 GHz processor and 16 GB RAM. The ode23tb solver is used for system integration, as it is well suited for switched power electronic circuits with stiff dynamics. A fixed-step size of 1 µs is employed to accurately capture the high-frequency switching of the converter operating at 10 kHz. The total simulation time is set to 1s, which includes the transient and steady-state operating conditions. All control algorithms are implemented using MATLAB embedded functions, while power electronic components are modelled using Simscape Electrical blocks. Table 1 represents specification of parameter for proposed work.

Table 1. Specification of parameters

	Parameters	Specification						
Fuel Cell								
Volta	ge at1 A and 0 A	[63,65]						
Nomin	al operating point	[133.3 ,45]						
Maximi	ım operating point	[225,37]						
Nı	imber of cells	65						
Nomin	al stack efficacy	55 %						
Nomi	nal air flow rate	300						
Nomin	al supply pressure	[1.5,1]						
Nome	inal composition	[99.95,21,1]						
Symbol	Description	Typical value	Unit					
A_1	Empirical constant (offset)	-0.9514	V					
A_2	Temperature slope	$+3.12 \times 10^{-3}$	V/K					
A_3	CO ₂ coupling	$+7.4 \times 10^{-5}$	V/K					
A_4	Current density slope	-1.87×10^{-4}	V/K					
High gain Landsman converter								
	L_1, L_2, L_i	4.7 <i>mH</i>						
	C_1, C_i	22 μF						
	\mathcal{C}_2	$2200~\mu F$						
Swite	ching frequency f	10kHz						

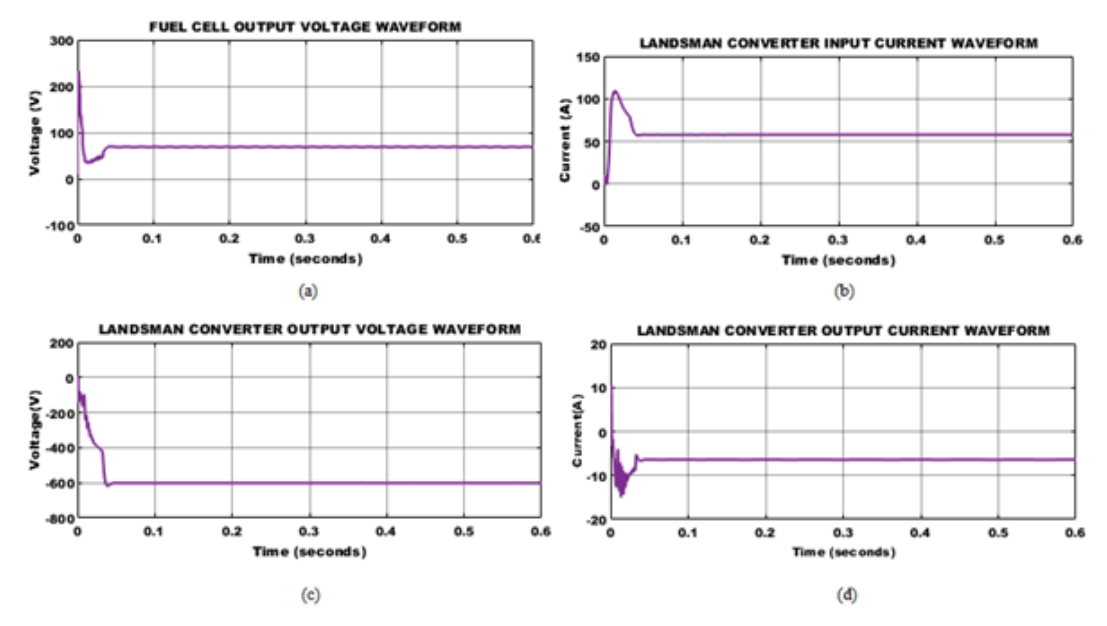


Fig. 9. Waveform of converter.

Figure 9(a) indicates the output voltage waveform of FC and it has variations in starting time. Finally, output voltage is sustained a steady value of 80 V with small fluctuations through the system. Input current is varied in initial period and is settled a constant value of 60 A as revealed in Figure 9 (b). Figure 9 (c) shows a output voltage, which has random

variations (starting period) and sustains a constant value of $-600 \, V$. Figure 9 (d) illustrates the converter's output current, which is varied in initial time and maintained at a constant value of $-7.5 \, A$ in the entire system.

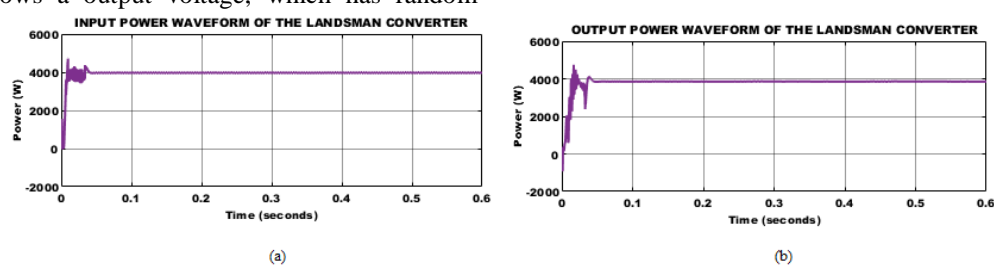


Fig. 10. Power waveform.

Figure 10 (a) and (b) represents input and output waveform of power. The converter's input power has some random fluctuations and continued a stable value of 4000 W.

Likewise, output power is initially changed and preserved at a constant value of 4300W through the system.

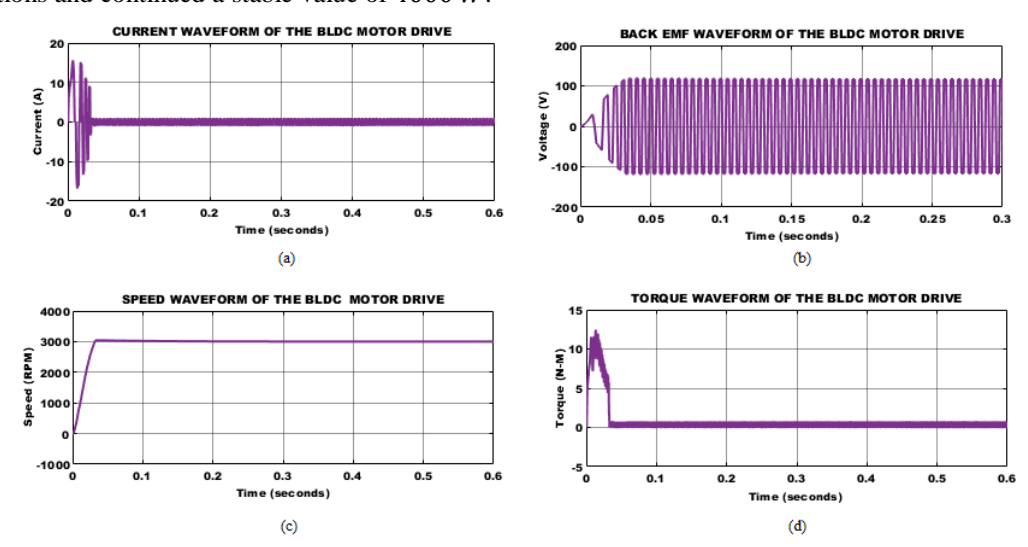


Fig. 11. Waveform of BLDC motor.

Figure 11 (a) illustrates the BLDC motor's current waveform, which has random variations in starting period and finally sustains a steady value of 3A in the entire system. Back EMF of BLDC motor is altered in initial period and maintained at a steady value of $110\ V$, as seen in Figure 11 (b). The speed waveform of BLDC motor is presented in Figure 11 (c), which is varied and is sustained a stable value of $3000\ RPM$. Figure 11 (d) exhibits torque waveform of BLDC motor, which has some changes in starting period and finally sustained a value of $1\ N-M$ in the entire system.

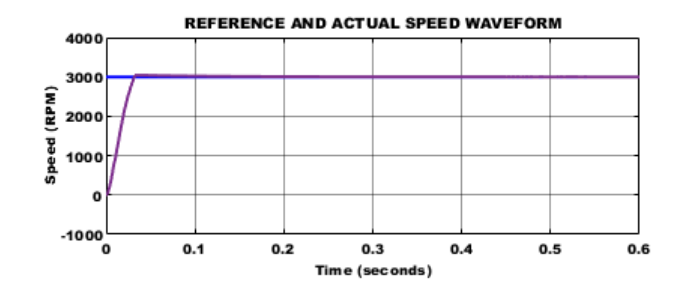


Fig. 12. Speed waveform.

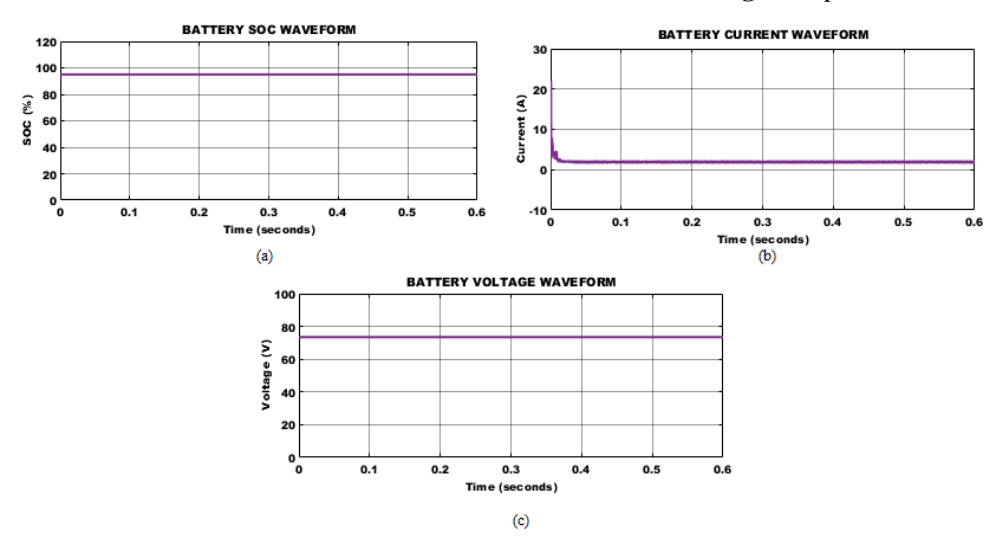
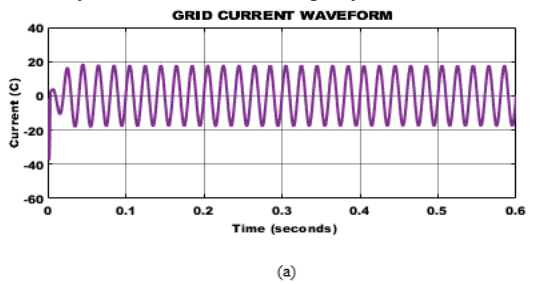


Fig. 13. Battery waveforms.

The waveform of reference and actual speed is seen in Figure 12, which has changes in initial period and preserved a stable value of 3000 *RPM*. Figure 13 (a) indicates the battery State of Charge (SOC) waveform and it has stable value of 95 %. The battery current value is slightly transformed in

early period and is maintained a constant value of 2A throughout the system, as represented in Figure 13 (b). Figure 13 (c) reveals the voltage waveform of battery, which is continued at a value of 75 V.



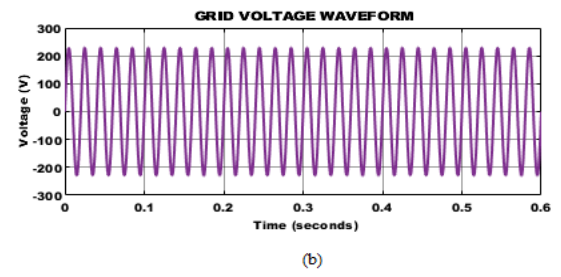
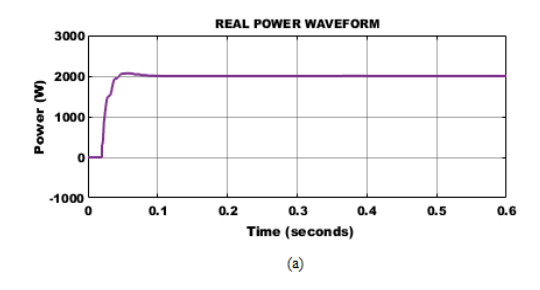


Fig. 14. Grid waveforms.

At first, current waveform of grid is slightly varied and continued a stable value of 18 A as indicated in Figure 14 (a).

Grid voltage waveform is revealed in Figure 14 (b), which sustains the persistent value of 210 *V* in the entire system.



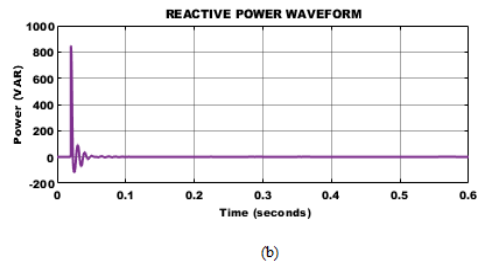


Fig. 15. Waveform of power.

INTERNATIONAL JOURNAL of SMART GRID V. Suresh et al., Vol.9, No.3, September, 2025

Figure 15(a) and (b) is displayed a waveforms for real and reactive power. Reduced reactive power leads to greater real power performance because it allows for more effective use of the system's active power, resulting in improved total power efficacy. Figure 16 represents in-phase voltage and current, in which voltage of grid is continued a stable value of 210 V and grid current is 18 A.

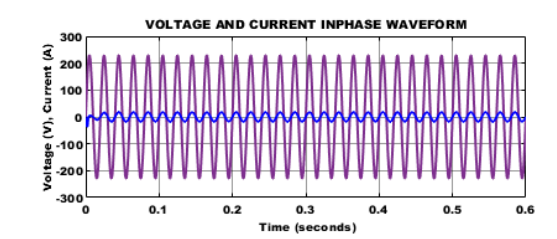


Fig. 16. Waveform of inphase voltage and current.

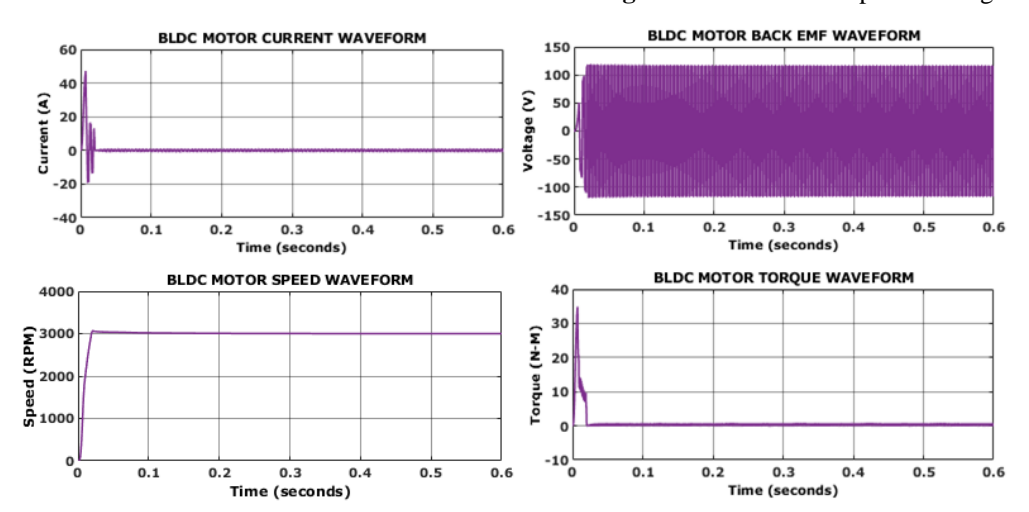


Fig. 17. BLDC motor response during under low load condition.

Figure 17 indicating the dynamic behavior of the motor under load condition, show that the phase current has an initial peak of $\pm 40~A$ before settling down at 10A, a steady state level in 0.03 s. The back EMF waveforms show that it has reached steady state at an amplitude of the order of $\pm 120~V$, correctly performed after the transients has passed. The motor speed comes up to the reference of around 3000~RPM very quickly, and has a slight overshoot, which returns back to steady state at 0.1 s. Electromagnetic torque also shows that motor has had an initial peak of nearly 35~N.~m to overcome the sudden load condition, and has n returned to close to 1~N·m by 0.08 s. The results demonstrate that the STO tuned PI controller enables fast settling, minimal overshoot and stable behavior of the BLDC motor operating during transient conditions.

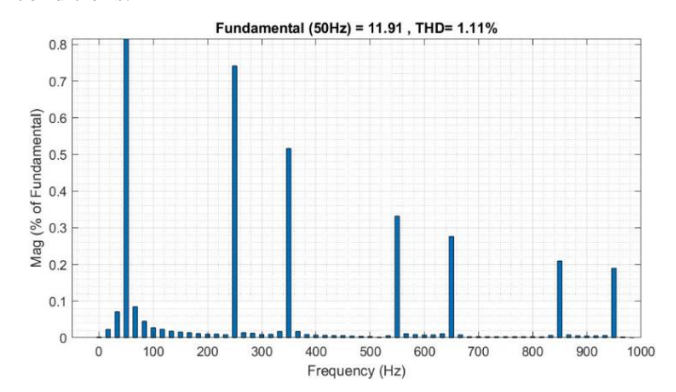


Fig. 18. Waveform of THD.

Figure 18 shows the THD value of 1.11%, which evaluates the frequency-dependent incidence of harmonic frequencies in a voltage signal. A THD of 1.11 % indicates the harmonic elements constitute a minor part of an entire current

waveform, demonstrating effective power transmission and better quality.

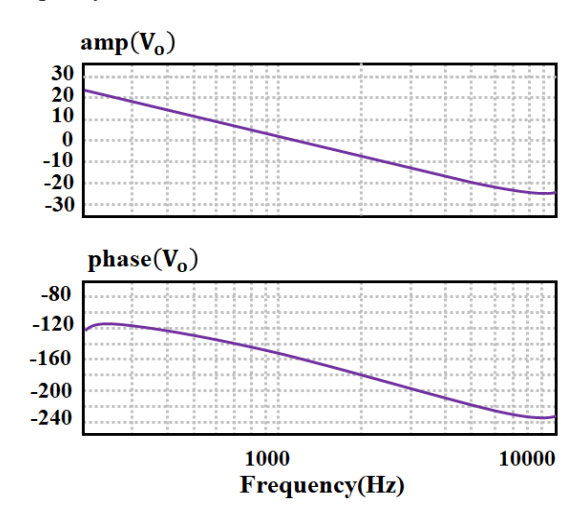


Fig. 19. Bode plot for the STO-tuned PI controller.

Figure 19 displays the Bode plot for the STO-tuned PI controlled converter system. The magnitude plot indicates a gain crossover frequency and the phase plot indicates a phase margin of degrees. The positive values for phase margin and gain margin assure that the closed-loop structure stable under the designed STO-PI control. In addition, the gradual slope of the magnitude response signifies better robustness against high-frequency disturbances. This stability analysis confirms that the STO-tuned PI controller produce a suitable dynamic response while guaranteeing adequately high-loop stability. This justifies using the STO-tuned PI controller to regulate the FC based system.

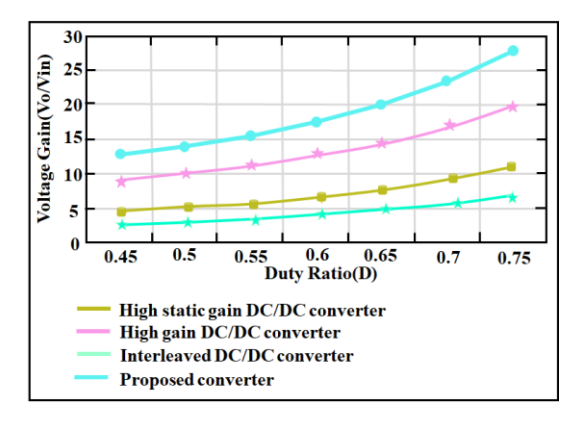


Fig. 20. Comparison of voltage gain.

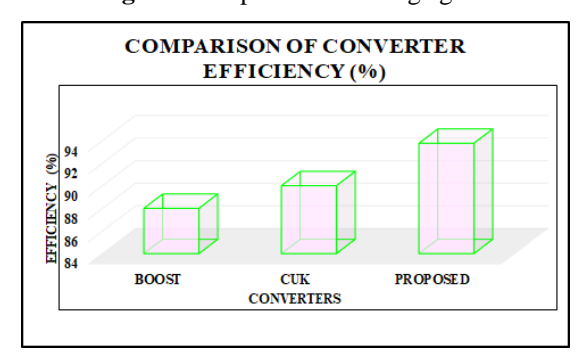


Fig. 21. Comparison of converter efficiency.

The voltage gain comparison for developed converter with distinct DC/DC converters is displayed in Figure 20. The high step-up converter [25], high static gain converter [26] and interleaved converter [27] have the lowest voltage gain than the proposed converter.

The comparison of efficacy for Boost [28], SEPIC [19] and developed converter is presented in Figure 21. The proposed converter achieves higher efficiency of 93.75% than Boost (88%) and SEPIC (90%) converters.

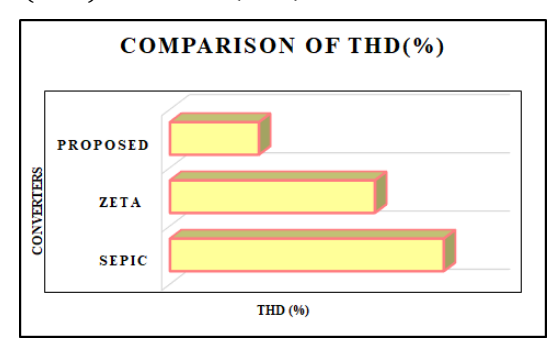


Fig. 22. Comparison of THD.

Figure 22 reveals the comparison of THD for developed converter with SEPIC [29] and Zeta [30] converters. The developed converter has the THD of 1.11%, which is better than SEPIC (3.42%) and Zeta (2.56%) converters.

Table 2. Comparison of Interleaved Landsman Converter (ILC) and proposed converter

Converter	switch	Diode	Capacitor	Inductor	Total components	Voltage gain	Efficiency
ILC [31]	2	2	3	4	11	=	91.5%
Proposed	1	4	3	3	11	$-\left(\frac{1+D}{1-D}\right)$	93.75%

Table 2 summarizes the converter design level comparison of the conventional ILC and the proposed High Gain Landsman Converter [31]. Both converters have a total of 11 components, whereas the proposed converter has an overall better design with only 1 active switch and a higher efficiency (93.75%) compared to the ILC (91.5%). In addition, it has a higher voltage gain which is beneficial for a high stepup converter.

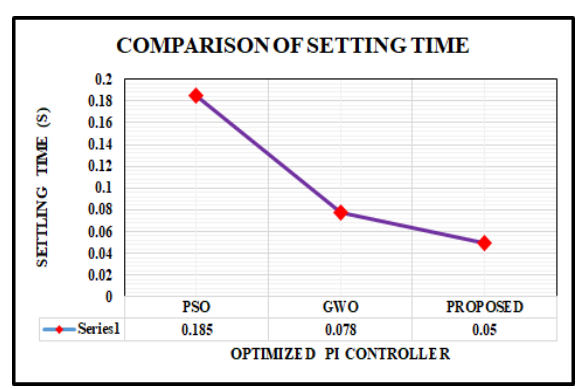


Fig. 23. Comparison of settling time.

Figure 23 provides a summary of settling time for the presented PI controller optimization methods where it seen that the proposed STO-PI controller had considerably lower

settling time (0.05 s) as compared to Grey Wolf Optimization (GWO) [32] (0.078 s) and PSO [33] (0.185 s), indicating a faster response of the system and a more effective method of optimization in terms of achieving dynamic performance.

The proposed algorithm is chosen instead of traditional methods such as PSO and GWO because it has faster convergence speed, less control parameters, and better ability of escaping local optima. PSO is frequently found to have slow convergence speed for high dimensional problems, while GWO is dependent on number of wolves and amount of iterations. The STO is able to set a good balance between exploration and exploitation based on its hunting and fighting strategies. From results, the STO-PI controller has a lower settling time (0.05 s) than GWO and PSO thus indicating its superiority in convergence and dynamic performance.

The outcomes proved that the proposed converter exhibits a higher voltage gain and efficiency than conventional Boost, SEPIC, and Zeta converters. The STO-tuned PI controller keeps the system stable in both the steady state and transient states and the SOC-based battery management system supports reliable energy balancing. These findings, demonstrate that the developed architecture successfully solves issues of low FC voltage, time-varying power demand, and power quality.

4. Conclusion

In this research, a FC-powered BLDC motor is proposed as an environmentally friendly power source for EVs. The FC's low voltage is enhanced by utilizing the developed high gain Landsman converter. The STO algorithm operates to adjust the parameters of a PI controller, which is designed to stabilise DC voltage of FCs. To store the FC's extra energy, battery is exploited, which delivers continuous supply to EV and battery's charging/discharging operation is performed by BDC converter. The entire research is applied in MATLAB/Simulink and comparison is made with traditional techniques to demonstrate prominence of developed research. It has been established as the researched work achieves better converter efficiency of 93.75% and THD of 1.11%. The obtained results show that the BLDC motor of an EVsis effectively powered by a FC.

References

- [1] F. Wu, B. Yang, A. Hu, Y. Zhang, W. Ge, L. Ni, C. Wang, and Y. Zha, "Inertia and damping analysis of gridtied photovoltaic power generation system with dc voltage droop control", in IEEE Access, vol. 9, pp. 38411-38418, 2021.
- [2] N. Tak, S. K. Chattopadhyay, and C. Chakraborty, "Single-sourced double-stage multilevel inverter for grid-connected solar PV systems", in IEEE Open Journal of the Industrial Electronics Society, vol. 3, pp. 561-581, 2022.
- [3] A. Kumar, and P. Kumar, "Power quality improvement for grid-connected PV system based on distribution static compensator with fuzzy logic controller and UVT/ADALINE-based least mean square controller", in Journal of Modern Power Systems and Clean Energy, vol. 9, No. 6, pp. 1289-1299, November 2021.
- [4] K. Sarita, S. Kumar, A. S. S. Vardhan, R. M. Elavarasan, R. K. Saket, G. M. Shafiullah, and E. Hossain, "Power enhancement with grid stabilization of renewable energybased generation system using UPQC-FLC-EVA Technique", in IEEE Access, vol. 8, pp. 207443-207464, 2020.
- [5] A. Bakeer, H. S. Salama, and I. vokony, "Integration of PV system with SMES based on model predictive control for utility grid reliability improvement", in Protection and Control of Modern Power Systems, vol. 6, no. 2, pp. 1-13, April 2021.
- [6] L. Yao, and J. C. Teo, "Optimal power dispatch for a chlorine factory with fuel cells participating in incentivebased demand response", in IEEE Transactions on Industrial Informatics, vol. 20, no. 3, pp. 4517-4526, March 2024.
- [7] B. Modu, M. P. B. Abdullah, A. Alkassem, H. Z. A. Garni, and M. Alkabi, "Optimal design of a grid-independent solar-fuel cell-biomass energy system using an enhanced salp swarm algorithm considering rule-based energy management strategy", in IEEE Access, vol. 12, pp. 23914-23929, 2024.

- [8] K. Hasan, M. M. Othman, S. T. Meraj, M. Ahmadipour, M. S. H. Lipu, and M. Gitizadeh, "A unified linear selfregulating method for active/reactive sustainable energy management system in fuel-cell connected utility network", in IEEE Access, vol. 11, pp. 21612-21630, 2023.
- [9] X. Chen, W. Cao, Q. Zhang, S. Hu, and J. Zhang, "Artificial intelligence-aided model predictive control for a grid-tied wind-hydrogen-fuel cell system", in IEEE Access, vol. 8, pp. 92418-92430, 2020.
- [10] H. Lee, and S. W. Cha, "Energy management strategy of fuel cell electric vehicles using model-based reinforcement learning with data-driven model update", IEEE Access, vol. 9, pp. 59244-59254, 2021.
- [11] J. Lee, and H. Lee, "Nonlinear model predictive control based adaptive equivalent consumption minimization strategy for fuel cell electric bus considering average travel speed", in IEEE Access, vol. 11, pp. 102605-102622, 2023.
- [12] K. P. Joshua, A. Manjula, V. Jegathesan, and S. Prabagaran, "Optimizing fuel cell power: an online energy management strategy for extended range in fuel cell hybrid electric vehicles", Environment, Development and Sustainability, pp. 1-23, 2024.
- [13] J. Zhou, C. Feng, Q. Su, S. Jiang, Z. Fan, J. Ruan, S. Sun, and L. Hu, "The multi-objective optimization of powertrain design and energy management strategy for fuel cell–battery electric vehicle", Sustainability,vol. 14, no. 10, pp. 6320, 2022.
- [14] Y. Belkhier, A. Oubelaid, and R. N. Shaw, "Hybrid power management and control of fuel cells-battery energy storage system in hybrid electric vehicle under three different modes", Energy Storage, vol. 6, no. 1, pp. e511, 2024.
- [15] K. Song, Y. Wang, C. An, H. Xu, and Y. Ding, "Design and validation of energy management strategy for extended-range fuel cell electric vehicle using bond graph method", Energies, vol.14, no. 2, pp. 380, 2021.
- [16] F. Akter, T. K. Roy, M. S. Islam, A. F. Alkhateeb, and M. A. Mollah, "Design of a nonlinear integral terminal sliding mode controller for a pem fuel cell based on a dcdc boost converter", IEEE Access, no.10, pp. 97419-97428, 2022.
- [17] M. Derbeli, O. Barambones, M. Y. Silaa, and C. Napole, "Real-time implementation of a new MPPT control method for a DC-DC boost converter used in a PEM fuel cell power system", In Actuators, vol. 9, no. 4, pp. 105. MDPI, 2020.
- [18] D. B. Aeggegn, G. N. Nyakoe, and C. Wekesa, "ANFIS-controlled boost and bidirectional buck-boost DC-DC converters for solar PV, fuel cell, and BESS-Based microgrid application", International Transactions on Electrical Energy Systems, vol. 2024, no. 1, pp. 6484369, 2024.

- [19] Z. Haider, A. Ulasyar, A. Khattak, H. S. Zad, A. Mohammad, A. A. Alahmadi, and N. Ullah, "Development and analysis of a novel high-gain CUK converter using voltage-multiplier units", Electronics, vol. 11, no. 17, pp. 2766, 2022.
- [20] S. Bairabathina, and B. S, "Design and validation of a SEPIC-based novel multi-input dc-dc converter for grid-independent hybrid electric vehicles", Energies, vol. 15, no. 15, pp. 5663, 2022.
- [21] I. Laoprom, and S. Tunyasrirut, "Design of PI controller for voltage controller of four-phase interleaved boost converter using particle swarm optimization", Journal of Control Science and Engineering, vol. 2020, no. 1, pp. 9515160, 2020.
- [22] A. H. Sule, A. S. Mokhtar, J. J. B. Jamian, A. Khidrani, and R. M. Larik, "Optimal tuning of proportional integral controller for fixed-speed wind turbine using grey wolf optimizer", International Journal of Electrical and Computer Engineering (IJECE), vol. 10, no. 5, pp. 5251-5261, 2020.
- [23] A. H. Gana, A. L. Amoo, G. A. Bakare, and A. A. Echo, "Load frequency control strategy for the nigerian power system using artificial bee colony optimized PI controller", World Wide Journal of Multidisciplinary Research and Development, vol. 7, no. 6, pp. 25-29, 2021.
- [24] I. Anshory, J. Jamaaluddin, A. Wisaksono, I. Sulistiyowati, B. S. Rintyarna, A. Fudholi, Y. A. Rahman, and K. Sopian, "Optimization DC-DC boost converter of BLDC motor drive by solar panel using PID and firefly algorithm", Results in Engineering, no. 21, pp. 101727, 2024.
- [25] W. Hassan, D. D. C. Lu, and W. Xiao, "Single-switch high step-up DC-DC converter with low and steady switch voltage stress", IEEE Transactions on Industrial Electronics, vol. 66, no. 12, pp. 9326-9338, 2019.
- [26] M. B. Meier, S. A. da Silva, A. A. Badin, E. F. R. Romaneli, and R. Gules, "Soft-switching high static gain DC–DC converter without auxiliary switches", IEEE Transactions on Industrial Electronics, vol. 65, no. 3, pp. 2335-2345, 2017.
- [27] S. Sathyan, H. M. Suryawanshi, A. B. Shitole, M. S. Ballal, and V. B. Borghate, "Soft-switched interleaved DC/DC converter as front-end of multi-inverter structure for micro grid applications", IEEE Transactions on Power Electronics, vol. 33, no. 9, pp. 7645-7655, 2017.
- [28] J. D. Navamani, K. Vijayakumar, and R. Jegatheesan, "Non-isolated high gain DC-DC converter by quadratic boost converter and voltage multiplier cell", Ain Shams Engineering Journal, vol. 9, no. 4, pp. 1397-1406, 2018.
- [29] K. S. Kavin, and P. Subha Karuvelam, "PV-based grid interactive PMBLDC electric vehicle with high gain interleaved DC-DC SEPIC Converter", IETE Journal of Research, vol. 69, no. 7, pp. 4791-4805, 2023.

- [30] L. P. Pattathurani, S. S. Dash, R. K. Dwibedi, M. D. Raj, R. Kannadasan, M. F. Savio, M. H. Alsharif, and J. H. Kim, "Harmonics minimisation in non-linear grid system using an intelligent hysteresis current controller operated from a solar powered ZETA converter", Sustainability, vol. 14, no. 12, pp. 7028, 2022.
- [31] R. Kushwaha, and B. Singh, "Interleaved landsman converter fed EV battery charger with power factor correction," IEEE Transactions on Industry Applications, vol. 56, no. 4, pp. 4179-4192, 2020.
- [32] M. Fodil, A. Djerioui, M. Ladjal, A. Saim, F. Berrabah, H. Mekki, S. Zeghlache, A. Houari, and M. F. Benkhoris, "Optimization of PI controller parameters by GWO algorithm for five-phase asynchronous motor," Energies, vol. 16, no. 10, pp. 4251.2023.
- [33] M. F. Roslan, A. Q. Al-Shetwi, M. A. Hannan, P. J. Ker, and A. W. M. Zuhdi, "Particle swarm optimization algorithm-based PI inverter controller for a grid-connected PV system," PloS one, vol. 15, no. 12, pp. e0243581, 2020.